University Library

MINERVA ACCESS

A gateway to Melbourne's research publications

Minerva Access is the Institutional Repository of The University of Melbourne

Author/s:
Shi, S;Lam, N;Cui, Y;Zhang, L;Lu, G;Gad, E

Title:
Indentation into an aluminium panel by the impact of a rigid spherical object

Date:
2022-11

Citation:
Shi, S., Lam, N., Cui, Y., Zhang, L., Lu, G. & Gad, E. (2022). Indentation into an aluminium panel by the impact of a rigid spherical object. Thin-Walled Structures, 180, https://doi.org/10.1016/j.tws.2022.109935.

Persistent Link:
https://hdl.handle.net/11343/311986

Revised Manuscript [Clean version]

Click here to view linked References

Indentation into an aluminium panel by the impact of a rigid spherical object

Shuangmin Shi[a]

[a] Department of Infrastructure Engineering, The University of Melbourne

Parkville, VIC, 3010, Australia. shuangmins@student.unimelb.edu.au

Nelson Lam[b*]

[b] Department of Infrastructure Engineering, The University of Melbourne

Parkville, VIC, 3010, Australia. ntkl@unimelb.edu.au

Yiwen Cui[c]

[c] Department of Infrastructure Engineering, The University of Melbourne

Parkville, VIC, 3010, Australia. yiwcui1@student.unimelb.edu.au

Lihai Zhang[d]

[d] Department of Infrastructure Engineering, The University of Melbourne

Parkville, VIC, 3010, Australia. lihzhang@unimelb.edu.au

Guoxing Lu[e]

[e] School of Engineering, Swinburne University of Technology, Hawthorn, VIC, 3122, Australia.

glu@swin.edu.au

Emad Gad[f]

[f] School of Engineering, Swinburne University of Technology, Hawthorn, VIC, 3122, Australia.

egad@swin.edu.au

[*]Corresponding author

Abstract

This paper introduces algebraic expressions for determining the amount of permanent indentation caused to an aluminium panel when impacted by a rigid spherical object. The magnitude of indentation is observed to vary significantly with the position of impact within the panel when the impactor and the velocity of impact are kept the same. This spatial variation of indentation is caused by the changes in the combinational mass (which is in turn function of the participating mass of the plate) and the Coefficient of Restitution COR. Both parameters are shown to correlate with the position of impact. The proposed algebraic expression featuring the combinational mass and COR as input parameters, allows potential damage to the panel to be predicted conveniently in day-to-day engineering practices. The original contribution of this article is in illustrating this phenomenon analytically, and have the analytical predictions verified by impact experimentation which has been conducted by the authors on panels of varying dimensions.

Keywords: Permanent indentation; Aluminium cladding; Impact; Projectile; Spatial variation

1. Introduction

Building facades and roofing panels can sustain considerable damage in bad weather. Much of the damage to metal storm panels as described is caused by hail and windborne projectiles. Thus, a reliable, and effective, method of predicting the extent of damage is warranted for given projectile impact scenario which is defined by the type of impactor, impactor mass and velocity of impact. The piercing action of a projectile impact into the surface of a metal panel can cause perforations as a certain impact intensity threshold is reached. The ensuing leakage of rainwater might cause colossal damage to building contents and to electrical equipment generating fire hazards [1, 2]. With a lower intensity of impact, the defaced (dented) panels requiring replacement would also add to the damage bill which can be up to tens of millions of dollars in a city in the aftermath of a severe storm [3-5].The impact action by a projectile is highly transient in nature. Thus, the damaging potential of this type of impact action cannot be represented by a prescribed equivalent static force, nor by an impact force that is derived by simply equating kinetic energy to elastic strain energy as stipulated by some codes of practice (e.g., [6]). Research on quantifying contact force by windborne debris and hailstones have been comprehensively studied in the past decade [7-11]. However, the indentation behaviour of the cladding panel has yet to be systematically investigated to fulfill the increasing interest from manufacturing industries.

The damage severity of a panel when subjected to the impact of hail, or windborne debris, is always a primary concern to manufacturers and property owners. Hailstone impact on steel roof sheeting causing damage such as indentation and crack formation, has been investigated and reported [12, 13]. The capacity of insulated panels or aluminium composite panels in resisting windborne projectiles have also been examined [14-16]. Research into aluminium alloy plates in response to impact of a solid object, on the other hand, was mainly centred around the perforation behaviour in conditions of high intensity impact [17, 18]. Relatively

little attention has been devoted to the performance of aluminium alloy panels (which are still commonly used in practice) in conditions of low intensity impact.

Numerical simulations by sophisticated finite element software packages can be used to predict the deformation behaviour of a panel under impact actions in order to offer engineers the option to circumvent dynamic testings [19-23]. However, numerical simulations have the drawback of not providing realistic, and reliable, predictions of impact inflicted permanent indentation into a metal surface, as the accuracy of the simulations would rely heavily on the meshing of the contact region and the assumed dynamic properties of the impactor and target [24]. In addition, a disproportionately high computational time is required for execution even though the panel which is subject to analysis has simple geometry and support conditions. The issue with lengthy execution of the software is compounded with the need to undertake repetitive executions for ensuring convergence of results, and for tracking trends and sensitivity to change in values of the input parameters. An analytical approach to the prediction which has been validated experimentally is therefore preferred for use in day-to-day engineering practices.

An analytical expression based on energy principles which was originally developed by Duffey [25], has been refined over the years for predicting the amount of permanent indentation into an aluminium alloy by incorporating the strain hardening behaviour of the aluminium [26-28]. The challenge with employing the developed relationship is the need to accurately identify the amount of energy that has been transformed to cause indentation into the surface of the aluminium. This transformed energy is only a fraction of the kinetic energy that is delivered by the impact of the projectile. Taking the delivered energy as the transformed energy can grossly overstate the amount of permanent indentation for a given impact scenario.

An attempt to improve the abovementioned analytical model for predicting permanent indentation into aluminium, overcoming the challenges as described, was made by Pathirana,

et al. [29]. The attempt was a success in view of good agreement between the predicted and measured results, but the cited reference only deals with impact at the centre of a rectangular panel. Results from impact testing (which involved accelerating a projectile onto the specimen of an aluminium cladding by use of the gas gun) revealed varying amount of permanent indentation as the position of impact within the plate was changed when the impactor and the incident velocity of impact were both kept the same. No analytical model to explain this variation has been reported in the literature. Research into the observed change of indentation behaviour with the location of impact is very limited given that what has been reported in the literature most recently is mainly concerned with ballistic resistance of armour plates, and is not closely relevant to windborne debris which cruises at a much lower velocity [30, 31]. Recognising the need to address spatial variations in indentation, this article deals with predicting damage caused to the panel when impacted at different locations. The effect of the panel size on indentation behaviour is also investigated.

An overview of the methodology adopted to fulfill the aims of this study is shown in Figure 1. The theoretical development of the predictive analytical model is presented in Section 2. Experimental validation of the accuracy of the proposed predictive model is then presented along with a step-by-step illustration of the calculation procedure in Section 3 and 4.

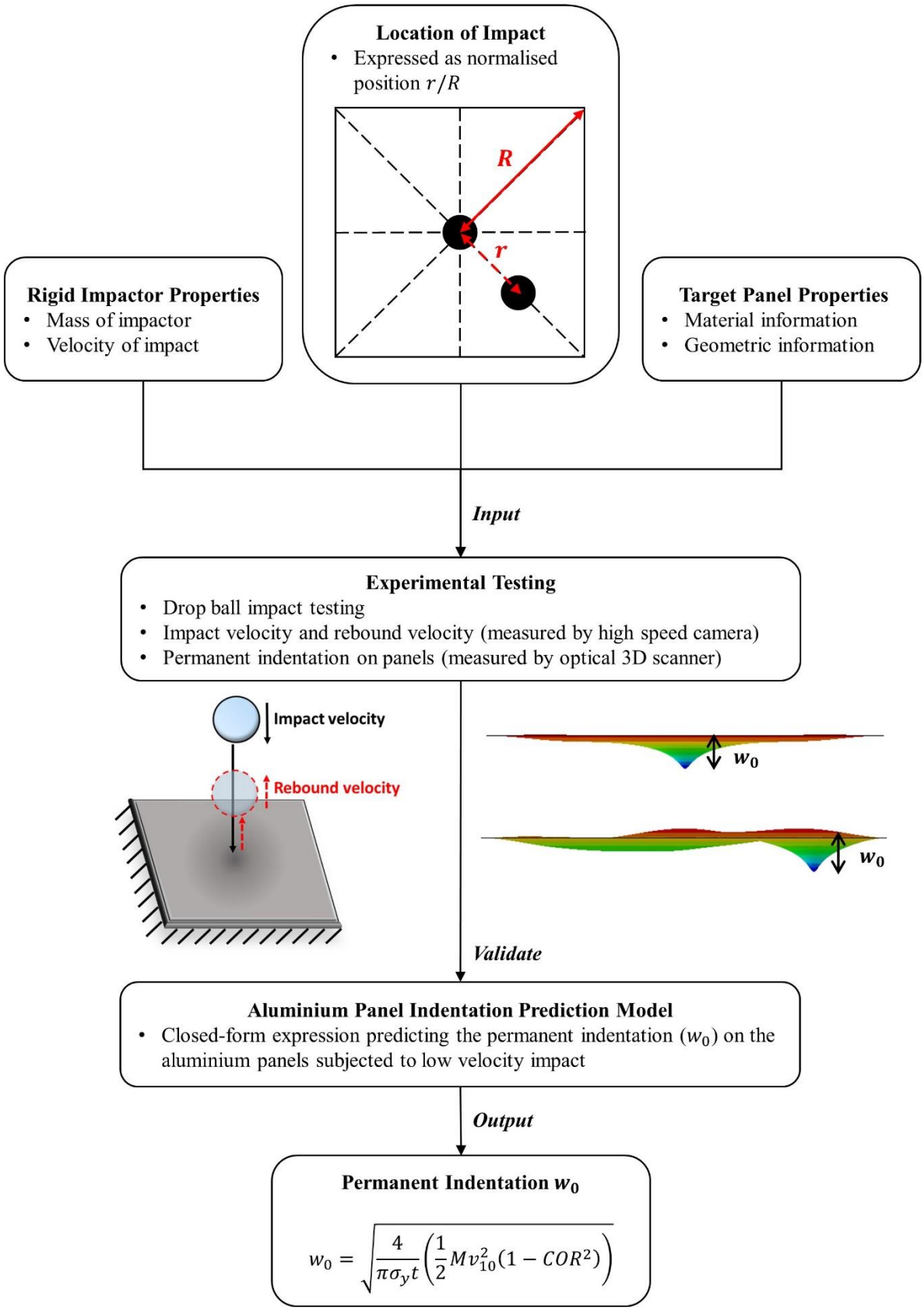


Figure 1: A schematic overview of the methodology used in this study

2. Underlying concepts of predictive methodology

2.1. Overview

An algebraic expression found on the principles of equating energy for predicting the amount of permanent indentation (w_0) on the surface of an aluminium panel was first derived by Duffey [25]. The total plastic strain energy responsible for causing permanent indentation (E_P^T) can be expressed as the volume integral of the sum of the product of radial and circumferential stresses and strains, based on thin plate theory and the assumption of plane stress and symmetric conditions (i.e., the *Kirchhoff* assumption), as presented in Eq. (1).

$$E_P^T = \int_{vol}[\int(\sigma_r d\varepsilon_r + \sigma_\theta d\varepsilon_\theta)]\, dV \qquad (1)$$

where, E_P^T is the amount of energy expended on causing indentation, and σ_r, σ_θ, ε_r, and ε_θ are the stresses and strains in the radial and circumferential directions respectively.

Assuming that circumferential strains equal to zero (i.e., $\varepsilon_\theta \approx 0$) based on Duffey [25], contributions from the second term of the integrand in Eq. (1) can be neglected. Following the incorporation of non-linear strain hardening behaviour of the aluminium material, the radial stress is assumed to take the following form: $\sigma_r = (\sigma_y + B\varepsilon_r^n)$, where σ_y is the initial yield stress, B and n are strain hardening material constants from the Johnson-Cook material model [28]. The derivation of the expression for predicting permanent indentation (w_0) is accordingly presented as follows.

$$E_P^T = 2\pi t \int_0^R \left(\sigma_y \varepsilon_r + \frac{1}{2} B\varepsilon_r^{n+1}\right) r dr \qquad (2)$$

where, t is thickness of the plate.

Radial strain ε_r can be predicted using Eq. (3) the proof of which is given by Duffey [25].

$$\varepsilon_r = \frac{1}{2}\left(\frac{\partial w(r)}{\partial r}\right)^2 \quad (3)$$

where, $w(r)$ is the deflection at radius r from the origin of the cylindrical coordinate system which can be approximated as $w(r) = w_0 e^{-r}$.

Substituting Eq. (3) into Eq. (2), results in Eq. (4) [29].

$$w_0^2\left[1 + \frac{a^{2n}B}{2^{n+1}\sigma_y(n+1)^2} w_0^{2n}\right] = \frac{4}{\pi\sigma_y t}(E_P^T) \quad (4)$$

where a is a constant.

It is noted that the term $\frac{a^{2n}B}{2^{n+1}\sigma_y(n+1)^2} w_0^{2n} \ll 1$ for aluminium alloy. Thus Eq. (4) can be simplified further and expressed in terms of w_0, as shown in Eq. (5).

$$w_0 = \sqrt{\frac{4}{\pi\sigma_y t}(E_P^T)} \quad (5)$$

The energy term E_P^T in Eq. (5) refers to the energy that is expended in causing indentation into the plate, which is not to be confused with the kinetic energy delivered by the impact. In the rest of this article, the r and R parameters as illustrated in Figure 2 will be used to define the location of impact within the targeted panel.

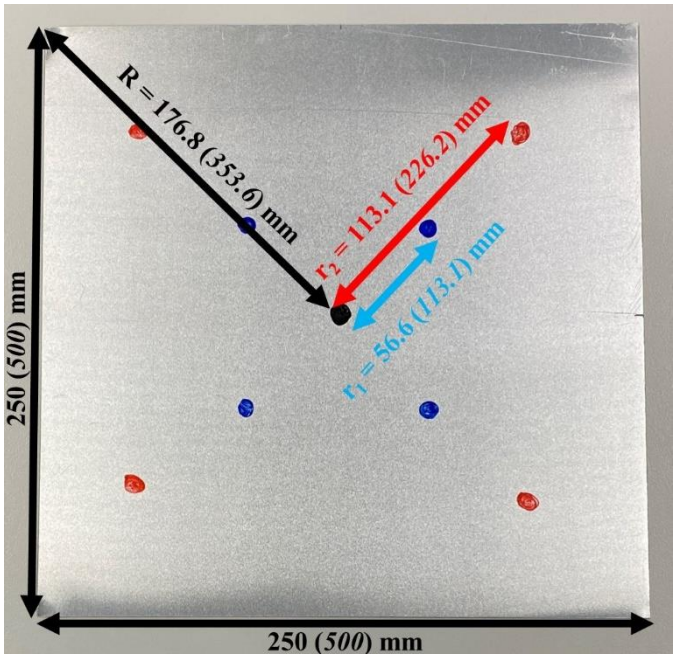


Figure 2: Varying impact locations on a tested panel of planar dimensions 250 mm × 250 mm (*500 mm* × *500 mm*) defined by r and R

In the following sub-section, an analytical model is presented to explain how the kinetic energy delivered by the impactor is transformed into different forms of energy, and how the distribution of energy varies with the position of impact as defined by the r/R ratio.

2.2. Energy absorbed by the deforming panel

The analytical model presented in below goes through the physical process of the collision in details for the purpose of deriving the mathematical relationship for resolving the distribution of energy into different forms. The time instance when the impactor first makes contact with the surface of the target (the cladding panel) marks the commencement of the compression phase of the impact action. At this instance, the initial velocity of the two colliding objects is denoted as v_{10} (for the impactor) and v_{20} (for the target). Once the two objects are in compression the amount of compressive contact pressure increases gradually until the maximum limit is reached. As the centre of the impactor is moving closer, and closer, to the surface of the target during the compression phase of the impact, the contact pressure continues

to increase. At the conclusion of the compression phase both the impactor and the target possess a common velocity of travel v_c. At the conclusion of the compression phase, the impact enters the restitution phase during which time the compressive pressure eases as deformation in the two bodies starts to restore. As this happens, the two objects start to move away from each other. At the conclusion of the restitution phase the two objects become separated. Their final velocities are denoted as v_{1f} (for the impactor) and v_{2f} (for the target). The velocity of motion of the two objects at different instances are shown in the schematic diagram of Figure 3 illustrating the two phases of the impact.

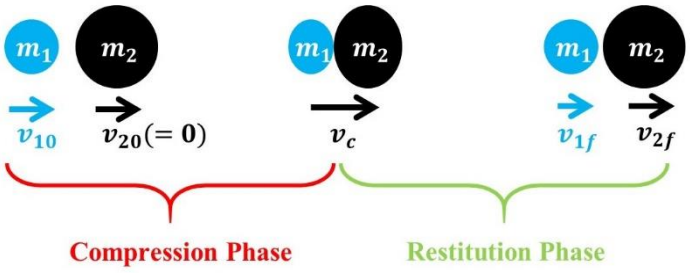


Figure 3: Schematic diagram of two phases during an impact action: compression phase & restitution phase

According to the law of conservation of energy, a relationship of the energy conversion within the system can be written in the form of Eq. (6).

$$E_0 = E_K^T + E_P^T + E_K^I + E_D^I + E_{loss} \quad (6)$$

where, E_0 is the kinetic energy delivered by the projectile ($=\frac{1}{2}m_1 v_{10}^2$), E_K^T and E_K^I are the kinetic energy of the target and the impactor at the end of restitution phase (as the colliding bodies start to separate), and are equal to $\frac{1}{2}m_2 v_{2f}^2$ and $\frac{1}{2}m_1 v_{1f}^2$, respectively, E_D^I is the energy dissipated within the impactor, E_P^T is the energy expended to cause permanent indentation into the aluminium plates, and E_{loss} is the energy dissipated in the form of sound, heat and friction.

Substituting the expressions of kinetic energy into Eq. (6) and rearranging it in terms of E_P^T, Eq. (7) can be obtained,

$$E_P^T = \frac{1}{2}m_1 v_{10}^2 - \left(\frac{1}{2}m_1 v_{1f}^2 + \frac{1}{2}m_2 v_{2f}^2\right) - E_D^I - E_{loss} \quad (7)$$

The expression for predicting the kinetic energy difference immediately prior to, and following, the impact can be simplified further into Eq. (8).

$$\frac{1}{2}m_1 v_{10}^2 - \left(\frac{1}{2}m_1 v_{1f}^2 + \frac{1}{2}m_2 v_{2f}^2\right) = \frac{1}{2}M v_{10}^2(1 - COR^2) \quad (8)$$

where, COR is the coefficient of restitution, M is the combinational mass of the system as defined by Eq. (9), and m_2 is the participating mass, of the targeted plate.

$$M = \frac{m_1 m_2}{m_1 + m_2} \quad (9)$$

Finally, the energy dissipated during the impact process in the form of sound, heat, and friction, which is characterised by the term E_{loss} [32], is caused by elastic waves generated within the object, and by Coulomb friction at the contact surfaces. Energy loss due to stress wave propagation in the plastic phase of the impact as investigated by Hutchings [33] was found to be very minor (only a few percent; < 3% of the kinetic energy). If permanent indentation is formed on the colliding surfaces, plastic deformation would be the dominant source of energy dissipation; energy loss due to Coulomb friction can therefore be neglected [34]. When neglecting the energy loss term E_{loss}, Eq. (7) can be rewritten into Eq. (10).

$$E_P^T = \frac{1}{2}M v_{10}^2(1 - COR^2) - E_D^I \quad (10)$$

The use of a rigid solid steel sphere as impactor in the example impact scenario as described has the advantage of minimising dissipation of energy through deformation within the sphere. As the Young's modulus of steel which the spherical impactor is made of is almost three times higher than the Young's modulus of aluminium which the targeted panel is made of, the amount

of energy dissipation within the steel sphere (E_D^I) is minor and can be assumed to be close to zero. Thus, indentation into the target can be observed with better clarity. By substituting Eq. (10) into Eq. (5) whilst neglecting E_D^I, an algebraic expression for estimating the amount of permanent indentation into the surface of the aluminium panel, taking into account spatial variation of M, is derived as shown by Eq. (11).

$$w_0 = \sqrt{\frac{4}{\pi\sigma_y t}(E_P^T)} = \sqrt{\frac{4}{\pi\sigma_y t}\left(\frac{1}{2}Mv_{10}^2(1-COR^2)\right)} \quad (11)$$

Both M and COR are key unknowns to be resolved for input into Eq. (11) for predicting w_0. Determination of the two parameters is dealt with in Section 2.3 and 2.4, respectively.

2.3. Participating Mass and Combinational Mass

The combinational mass as defined by Eq. (9), which is function of the impactor mass (m_1) and participating mass of the target (m_2), is introduced as a parameter to help determine the fraction of energy that is expended in causing indentation to the panel. It is inferred from Eq. (9) that as the value of m_2 is increased to a very large value, the value of M converges to that of m_1. As implied by Eq. (11), in an idealised impact scenario where the rigid impactor is accelerated onto the surface of a target of infinite mass, the initial kinetic energy delivered by the impact would be absorbed totally by the plate in the form of indentation (i.e., $M \sim m_1$ as m_2/m_1 tends to infinity) if assuming $COR \approx 0$. Consider a similar, but modified, scenario where the mass of the target is reduced to that of the impactor (i.e., $m_1 = m_2$). The amount of kinetic energy which is transformed into energy causing indentation (E_P^T) is reduced to 50% of the initial kinetic energy delivered by the impact, as the combination mass M is reduced to $0.5m_1$ (according to Eq. 9). The remaining 50% of the energy is transformed into kinetic energy generated by the motion of the target. Energy of this form will be dissipated eventually in the course of vibration of the plate. Details of energy conversion during the phase of free

vibration of the target will not be discussed herein, as the study is instead focused on the phase: from the start of compression to the end of restitution (which normally lasts for a few milliseconds only). As illustrated in the scenarios described above, when the value of m_2 (hence M) is decreased, the amount of energy expended to cause indentation is diminished accordingly. In a range of impact scenarios (involving the same impactor and velocity of impact applied to a rectangular plate of a finite size), the value of m_2 (hence M) which controls the amount of indentation is shown to be highly dependent on the location of the impact. This is an original discovery that can be illustrated analytically, and validated experimentally, as presented in the later sections of the article.

A common way of simplifying a plate element (which is targeted for a solid object impact) is having it reduced into an equivalent single-degree-of-freedom (SDOF) lumped mass system. The value of the participating mass (m_2), of a simply supported rectangular plate in free vibration has been found to be approximately ¼ of the total mass of the plate (M_{plate}) [35-37]. It is cautioned herein that the quoted *rule-of-the-thumb* is only valid for a plate undergoing free vibration. Results from impact experimentation (to be reported in the later part of this article) show that the actual value of m_2 can deviate significantly from predictions by the described *rule-of-the-thumb*, and is sensitive to the location of impact.

An inexpensive method of determining the value of m_2 is by conducting a simple experiment which involves striking the plate with a dropped rigid object, and then observing the motion behaviour of the tested objects. The underlying principles of the methodology as described herein is based on idealising the target as a lumped mass (m_2) which is supported on a spring. By the conservation of momentum principles, the change in momentum of the rigid impactor prior to, and immediately following, the impact can be equated to the amount of momentum transferred to the target (the plate). This approach of determining the value of m_2 is represented

algebraically by Eq. (12a). Rearranging Eq. (12a) into Eq. (12b) gives the following expression for determining m_2.

$$m_1 v_{10} = m_1 v_{1f} + m_2 v_{2f} \quad (12a)$$

$$m_2 = \frac{m_1(v_{10} - v_{1f})}{v_{2f}} \quad (12b)$$

where, m_1 is the mass of the impactor, v_{10} is the incident velocity of impact, and v_{1f} and v_{2f} is the velocity of the impactor and that of the idealised lumped mass, respectively, at the end of the restitution phase of the impact. The positive direction of the velocity is assumed to be the same as the direction of impact (i.e., the direction of v_{10})

In other words, the value of m_2 is equal to the change in momentum divided by the velocity recorded from the target lumped mass immediately following the impact.

The prototype model of the target is a plate which is deformable, whereas the idealised model which Eq. (12b) is based upon is a rigid lumped mass. In conditions of an impact scenario, deformation of the prototype (the plate) can be modelled as discrete finite elements, and with each element having its own tributary mass m_i and tributary velocity v_i. This dual model approach is illustrated by the schematic diagram of Figure 4. To achieve equivalence between the prototype and the lumped mass model the momentum and the kinetic energy generated from both systems are set the same through calibration, as shown in Eq. (13a) and Eq. (13b). Rearranging the two equations into Eq. (13c) gives the expression for determining the velocity v_{2f} of the equivalent single lumped mass system, being function of the array of v_i values defining the deflection profile of the plate in 3D.

$$\sum m_i v_i = m_2 v_{2f} \quad (13a)$$

$$\sum \frac{1}{2} m_i v_i^2 = \frac{1}{2} m_2 v_{2f}^2 \quad (13b)$$

$$v_{2f} = \frac{\sum m_i v_i^2}{\sum m_i v_i} = \frac{\sum v_i^2}{\sum v_i} \quad \text{for plate of uniform thickness} \quad (13c)$$

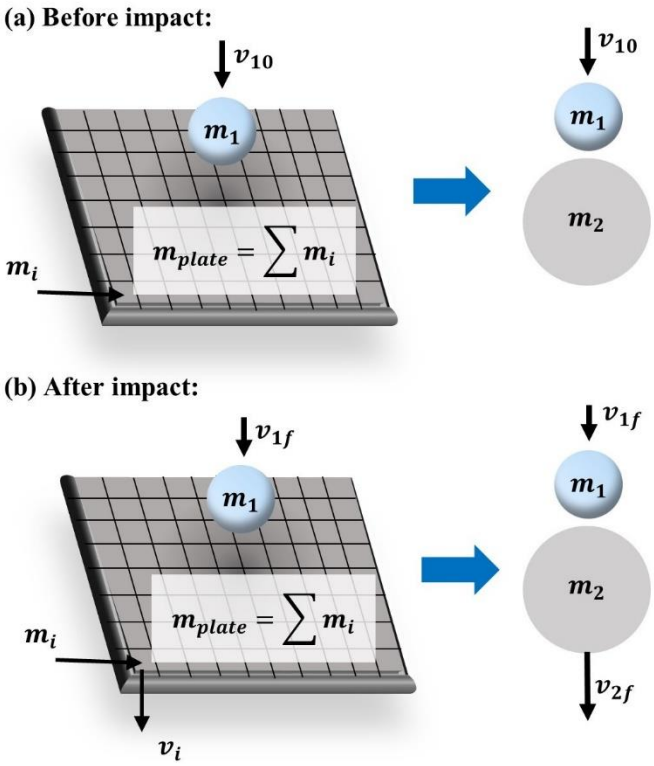


Figure 4: Equivalent single-degree-of-freedom (SDOF) structure for the plate structure (a) before impact (b) after impact

In order to obtain information in relation to the tributary velocity field v_i of all the finite elements of the plate structure, numerical simulations were implemented by the use of commercial software LS-DYNA. Initially, a homogenous aluminium plate 5050-H34 (with fully clamped edges) which was subjected to a low velocity impact of a 30 mm diameter steel ball cruising at a velocity of 3.13 m/s was modelled to validate the accuracy of the simulated results. The impact locations on the plate were chosen as $r/R = 0$, $r/R = 0.32$ and $r/R = 0.64$, as defined in Figure 2. The aluminium plate had dimensions of 250 mm × 250 mm × 1 mm thick and was modelled as planar shell elements with an element size of 1.0 mm × 1.0 mm to ensure the convergence of results. Material models MAT_020_RIGID and

MAT_018_POWER_LAW_PLASTICITY [38] have been employed to characterise the behaviour of the impactor and the target, respectively. The detailed material properties are as shown in Table 1. The contact behaviour between the projectile and the targeted object can be specified by the use of the following command: AUTOMATIC_SURFACE_TO_SURFACE [39]. The accuracy of the numerical model has been validated by the comparison of the displacement histories at different impact locations from simulations by LS-DYNA and from experimental measurements (Figure 5).

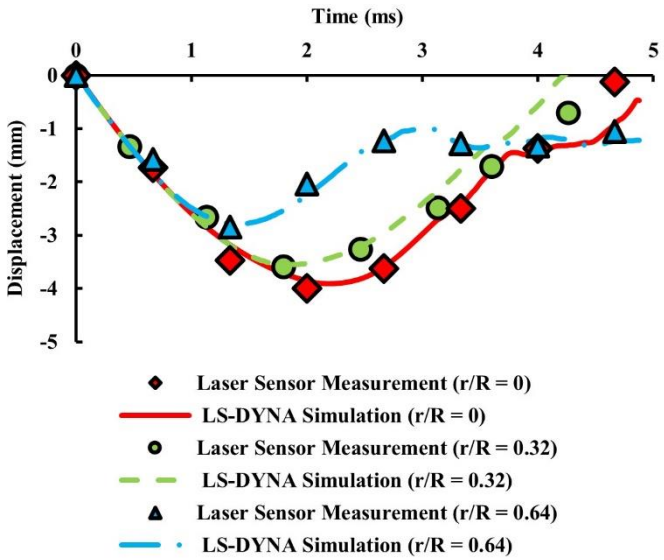


Figure 5: Comparison of displacement time histories at different impact locations (defined by the r/R ratio) measured from experiments and calculated by LS-DYNA

Similar simulation techniques have also been applied to a plate of dimensions 500 mm × 500 mm × 2 mm thick which was subjected to the same impact scenarios as described above. Convergence studies were performed to ensure that the adopted mesh elements would always achieve convergence. As shown in Figure 6, regardless of the plate planar dimensions, as the mesh size is reduced to 2 mm × 2 mm or smaller, the value of m_2 as calculated using Eq. (12b) would not vary significantly. The effects of changing boundary conditions have also been investigated by altering the edge restraints (from fully fixed to simply supported conditions). As shown in Figure 7 (a) and (b) the value of m_2 of a fully fixed plate would typically be the

same as, or slightly higher than, a simply supported plate. The difference in m_2 is generally minor when the location of impact is at the centre of the plate (i.e., r/R = 0).; but would increase as the location of impact moves closer to the boundary (i.e., as r/R becomes larger). As can be inferred from Eqs. (9) and (11), the magnitude of the permanent indentation (w_0) is directly proportional to the square root of the combinational mass (M) which would increase with the participating mass (m_2). Therefore, adopting a fully fixed boundary condition in the prediction of damage would translate to a higher margin of safety.

Table 1: Summary of material properties input for steel ball impactor and aluminium targeted plate used in LS-DYNA

Material properties of steel ball impactor (MAT_020) (ANSI/AFBMA Std. 10-1989)				
Density ρ (kg/m^3)	Young's modulus E (GPa)	Poisson's ratio ν		
7800	200	0.3		
Material properties of aluminium targeted plate (MAT_018) [40]				
Density ρ (kg/m^3)	Young's modulus E (GPa)	Poisson's ratio ν	Strength coefficient K (MPa)	Hardening exponent N
2700	69	0.33	254	0.0782

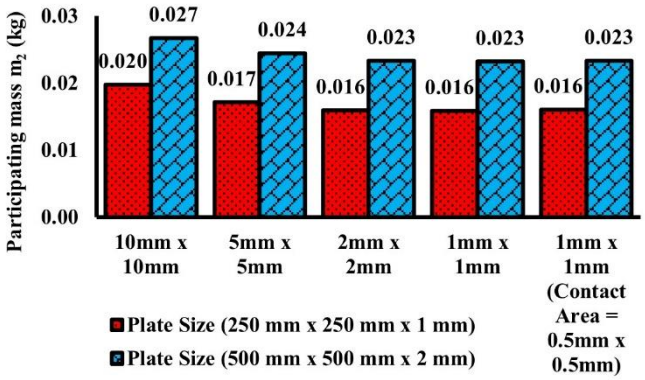
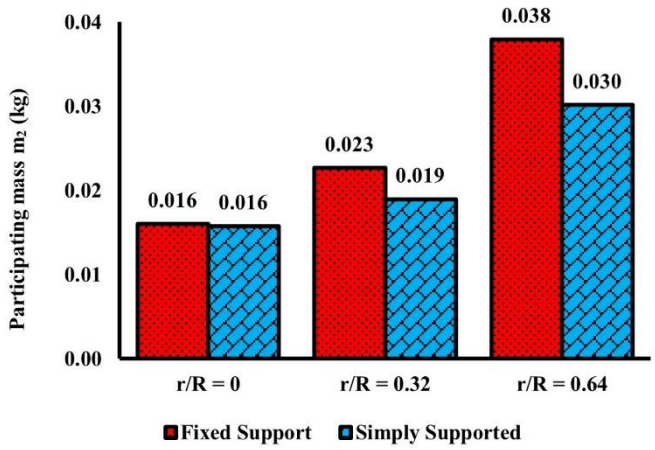
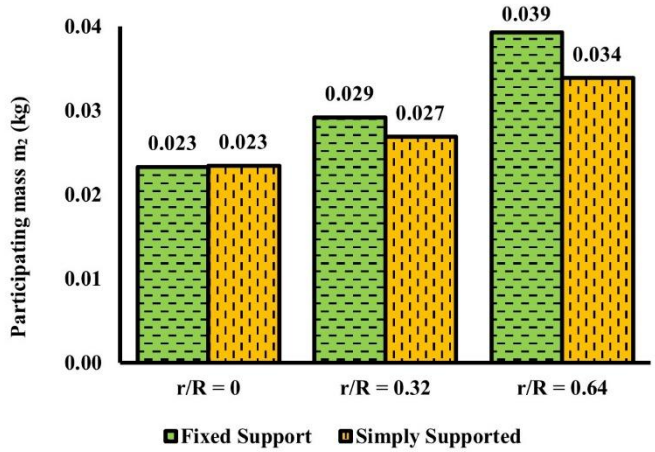


Figure 6: Convergence analysis of finite element models in LS-DYNA: effect of shell element size on the values of participating mass m_2



(a)



(b)

Figure 7: Sensitivity analysis of finite element models in LS-DYNA: effect of boundary conditions on the values of participating mass m_2 at different impact locations defined by the r/R ratio (a) 250 mm × 250 mm × 1 mm plate (b) 500 mm × 500 mm × 2 mm plate

Further simulations have been conducted by varying the diameter of the steel ball impactor from 30 mm to 40 mm, and 50.8 mm; and the velocity of impact from 3.13 m/s to 4.50 m/s, and 6.26 m/s. This simulation approach has been verified further in a later section of the paper where the amount of indentation as predicted by the proposed analytical relationship is compared against experimental measurements. The arrays of v_i values derived from the

simulations were input into Eq. (13c) for determining the value of v_{2f} which in turn were input into Eq. (12b) for solving the value of m_2.

It was found from the simulations that the velocity of the plate at the location of contact (denoted herein as v_n), was constrained to 0.77 – 0.94 times the value of v_{2f} as calculated using Eq. (13c). The v_n/v_{2f} ratio tends to be lower when moving closer to the centre of the plate, but becomes higher when moving towards the corner. When the location of impact was in the vicinity of the corner of the plate (e.g., r/R = 0.64) v_n came within 7 % of v_{2f}. These observations, which were consistent across different velocities of impact, can be used in the future to infer the value of v_{2f} when only v_n has been measured, thus sparing the need to perform the whole plate analysis. In other words, taking $v_{2f} = v_n$ would err on the conservative side in the prediction of w_0, and would only slightly overstate m_2.

In summary, the combined use of Eq. (12b) and Eq. (13c) enables the value of m_2 to be found once the following information is available: (1) impactor mass, m_1 (2) velocity of the impactor at different stages of the impact: v_{10} and v_{1f}, and (3) the array of velocity values v_i defining the deflection plate. Once the value of m_2 is known, the value of M of the impactor-plate system can be solved using Eq. (9). Substituting M into Eq. (11) returns the predicted value of w_0.

2.4. Coefficient of Restitution

The *Coefficient of Restitution* (COR) is used to characterise energy recovery during the restitution phase of the impact (refer Figure 3). COR as a modelling parameter may be defined in a number of ways. The three most common definitions are: (1) the kinetic coefficient of restitution which is ratio of the impulse transferred across two colliding bodies in the compression and restitution phase, (2) kinematic coefficient of restitution which is ratio of the relative velocity of the two colliding bodies immediately prior to, and following, the occurrence

of impact, or (3) energetic coefficient of restitution which is ratio of the strain energy of absorption and release in the compression and restitution phase, respectively. These three definitions which have been reviewed in [41] are presented in the mathematical expressions of Equations (14a) - (14c), respectively.

$$COR = \frac{p_r}{p_c} = \frac{\int_{t_c}^{t_f} F(t)dt}{\int_{t_0}^{t_c} F(t)dt} \quad (14a)$$

$$COR = \frac{v_{2f} - v_{1f}}{v_{10} - v_{20}} \quad (14b)$$

$$COR = \sqrt{\frac{E_r^e}{E_c^{ep}}} \quad (14c)$$

where, p_r and p_c are restitution impulse and compression impulse; t_0, t_c and t_f are the time instants of the start of the compression phase, the end of the compression phase and the end of restitution phase respectively; $F(t)$ is the contact force between the two bodies; E_r^e is the elastic strain energy restored during the restitution phase; and E_c^{ep} is the energy dissipated during the compression phase due to both elastic and plastic deformations.

Whilst there are different definitions of COR, their respective values are typically similar [42]. Should the deformation of the impactor and surface of the target be purely elastic (i.e., $COR = 1$), all the strain energy developed in the compression phase be transformed back into kinetic energy which is carried by both objects which move away from each other. In such a condition, the amount of permanent indentation occurring at the point of contact would be limited. Should there be negligible amount of recovery of strain energy in the restitution phase of the impact (i.e., $COR = 0$), the two colliding objects remain attached. In such a condition, a significant amount of indentation is expected to occur in the plate than the condition of elastic impact. In the current study, the kinematic coefficient of restitution definition is used and simplified into Eq. (15).

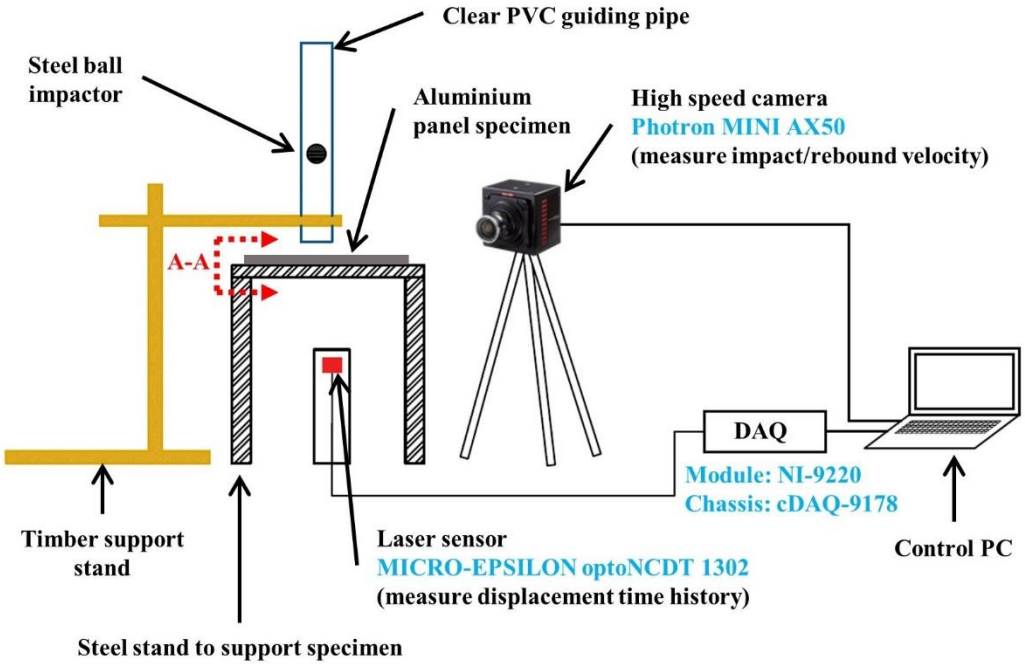
$$COR = \frac{Rebound\ velocity}{Impact\ velocity} = \sqrt{\frac{Rebound\ height}{Drop\ height}} \quad (15)$$

3. Experimental Investigation

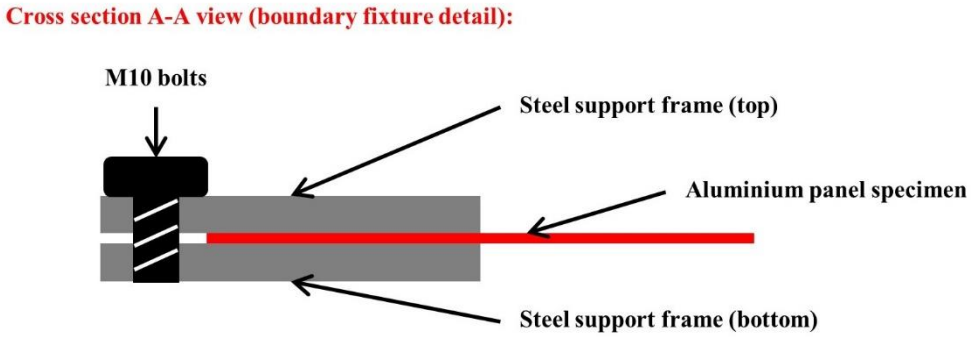
3.1. Experimental setup and test parameters

Predictive expressions presented in Section 2 for determining permanent deformation of the plate are evaluated in this section based on analyses of results from impact experiments conducted by the authors. The spatial dependent parameters: m_2 and COR were of key interests in the investigation as the amount of indentation into the plate is greatly influenced by these two parameters.

Impact tests which involved dropping a solid steel sphere onto an aluminium plate was conducted by the authors. The test setup as illustrated by Figure 8, along with photos of Figure 9, features the use of a PVC pipe to guide the fallen object onto various designated positions on a plate specimen which had plan dimensions of either: (1) 250 mm × 250 mm or (2) 500 mm × 500 mm. The plate thickness was 1 mm with the smaller plate and either 1 mm or 2 mm with the larger plate. The boundary of the targeted panel was fully clamped by two steel support frames and fixing bolts as illustrated in Figure 8(b). This type of boundary condition can be approximated as fully fixed support since both displacement and rotation at the support were restrained. The solid steel sphere had mass of 110 grams, 260 grams or 535 grams, as listed in Table 2. Physical properties of the test specimens were as listed in Table 2. The impact velocity of impact was (1) 3.13 m/s, (2) 4.5 m/s and (3) 6.26 m/s as measured by a high-speed camera (*Photron MINI AX50*) which was also used to measure the velocity of rebound. A laser device (*MICRO-EPSILON optoNCDT 1302*) and associated data acquisition system (DAQ) for recording the displacement time-history was placed under the specimen.



(a)



(b)

Figure 8: Schematic diagrams of (a) experimental setup (b) details of the fixture at boundary locations

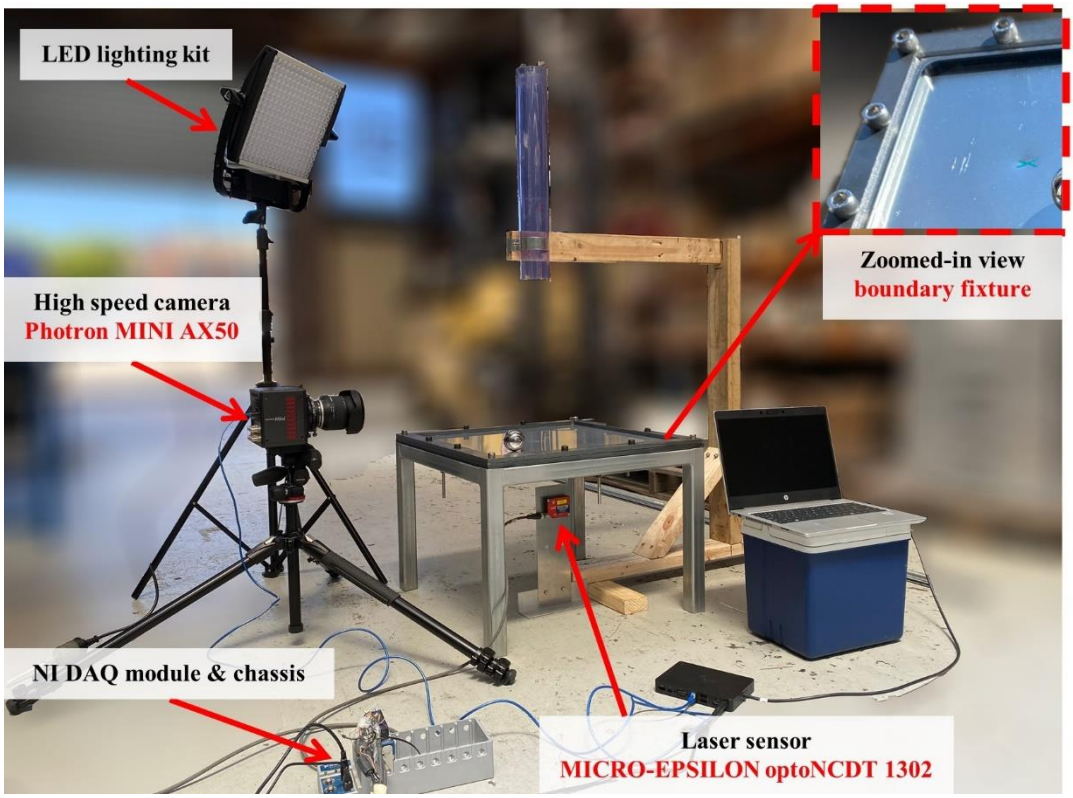


Figure 9: Photograph of experimental setup and instrumentations for measurement

Table 2: Dimensions and material properties of E52100 chrome steel ball impactor (ANSI/AFBMA Std. 10-1989)

	Impactor Type I	Impactor Type II	Impactor Type III
Diameter (mm)	30	40	50.8
Mass m_1 (g)	110	260	535

Table 3: Dimensions and material properties of targeted aluminium panels grade 5050-H34 (ASTM B209M standard)

	Panel Type I	Panel Type II	Panel Type III
Dimensions (mm)	250 × 250 × **1(*THK*)**	500 × 500 × **1(*THK*)**	500 × 500 × **2(*THK*)**
Yield strength σ_y (MPa)	140	140	140

3.2. Discussion of experimental results

3.2.1. Participating mass m_2

In determining the value of m_2 for every considered test scenario, impact experiments and numerical simulations were conducted to obtain measurements of the velocities taken from both the impactor and the targeted plate. Parameters characterising each of the impact tests including the size of the impactor, size of the test specimens, the velocity of impact and the location of impact are listed in Tables 4a and 4b. The participating mass ratio λ is also introduced herein as defined in Eq. (16).

$$\lambda = \frac{m_2}{m_1} \tag{16}$$

The increase in value of λ (i.e., the ratio of m_2/m_1), with increasing offset of the impact location from the centre of the plate is notable; so is the insensitivity of the ratio with change in velocity of impact. As shown in Table 4a, the value of λ would not change significantly with the increase in the velocity of impact when other parameters remain unchanged. The trend of increase in λ with increasing r/R is evident in Figure 10. Linear correlations of the value of λ with the location of impact can also be approximated for plates of two different thicknesses (1 mm and 2 mm) as shown in Figure 10(a) and (b) respectively. Such linear correlations as reflected in Eqs. (17a) and (17b) are applicable for locations along the diagonals as defined by r/R (refer Figure 2):

$$\lambda_1 = 0.316\left(\frac{r}{R}\right) + 0.135 \qquad \text{for plate of 1 mm thickness} \tag{17a}$$

$$\lambda_2 = 0.067\left(\frac{r}{R}\right) + 0.039 \qquad \text{for plate of 2 mm thickness} \tag{17b}$$

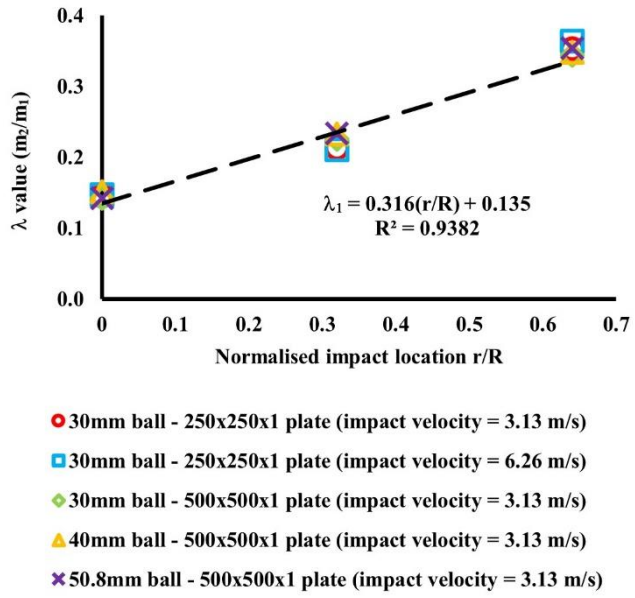
Table 4: Participating mass of the impact

(a) 250 mm × 250 mm × 1mm plate

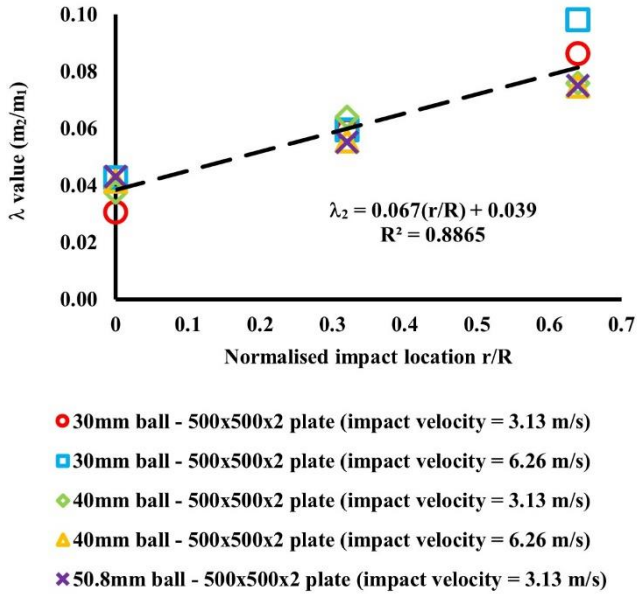
m_1 (g)	D (mm)	v_{10} (m/s)	*Impact location r/R*	v_{1f} (m/s)	v_{2f} (m/s) Eq.(13c)	m_2 (g) Eq.(12b)	λ
110	30	3.13	0.0	2.63	3.44	16.0	**0.146**
110	30	3.13	0.32	2.69	2.09	23.4	**0.213**
110	30	3.13	0.64	2.27	2.44	38.9	**0.353**
110	30	4.50	0.0	3.81	4.69	16.1	**0.147**
110	30	4.50	0.32	3.77	3.41	23.5	**0.214**
110	30	4.50	0.64	3.25	3.48	39.4	**0.359**
110	30	6.26	0.0	5.52	5.06	16.1	**0.147**
110	30	6.26	0.32	5.27	4.70	23.1	**0.211**
110	30	6.26	0.64	4.50	4.85	39.9	**0.364**

(b) 500 mm × 500 mm × 2 mm plate

m_1 (g)	D (mm)	v_{10} (m/s)	*Impact location r/R*	v_{1f} (m/s)	v_{2f} (m/s) Eq.(13c)	m_2 (g) Eq.(12b)	λ
261	40	3.13	0.0	3.02	2.92	9.8	**0.038**
261	40	3.13	0.32	2.94	3.01	16.6	**0.064**
261	40	3.13	0.64	2.92	2.77	19.8	**0.076**
261	40	6.26	0.0	6.04	5.30	10.8	**0.042**
261	40	6.26	0.32	5.97	5.23	14.5	**0.055**
261	40	6.26	0.64	5.85	5.55	19.5	**0.075**
535	50.8	3.13	0.0	3.00	3.01	23.0	**0.043**
535	50.8	3.13	0.32	2.97	2.90	29.4	**0.055**
535	50.8	3.13	0.64	2.96	2.27	40.0	**0.075**



(a)



(b)

Figure 10: Participating mass ratio λ (m_2/m_1) at different impact locations defined by r/R (a) plate of 1 mm thickness (b) plate of 2 mm thickness

3.2.2. *Coefficient of Restitution COR*

A separate parametric study was undertaken to study the spatial variation of COR, and its correlation with different impact parameters. It is observed from experiments that the value of COR would be decreased if the mass of the impactor, or the velocity of impact, is increased. The value of COR also tends to be a higher value when the impact occurs in closer proximity to the boundary of the plate, or when a thicker plate is impacted. In addition, COR is shown to be monotonically correlated with one parameter when other parameters remain unchanged, indicating the viability of having all the correlations to be covered by one expression.

To establish this expression, the technique of dimensional analysis was employed [43]. Two independent dimensionless groups were identified as COR and $(R-r)m_1v_{10}/\left(L^2\sqrt{\bar{m}D}\right)$. The latter term is referred as the dimensionless impact intensity which can be expressed in the form of Eq. (18a) which is product of two dimensionless variables.

$$\frac{(R-r)m_1v_{10}}{L^2\sqrt{\bar{m}D}} = \frac{R-r}{L} \times \frac{m_1v_{10}}{L\sqrt{\bar{m}D}} \tag{18a}$$

where, R and r are measurements of the impact location as defined by Figure 2 (and $R-r$ measures the distance from the impact location to the boundary); L is planar dimension of the targeted plate; $\bar{m}$ is mass per unit area of the plate; and D is flexural rigidity of the plate as defined by Eq. (18b)

$$D = \frac{Et^3}{12(1-\nu^2)} \tag{18b}$$

where, E, t, and ν are the Young's modulus, thickness, and Poisson's ratio of the targeted plate respectively.

In Eq. (18a), the first term $\frac{R-r}{L}$ is a dimensionless variable characterising the position of impact on panels of any given size L. The second term $\frac{m_1 v_{10}}{L\sqrt{\bar{m}D}}$ is another dimensionless variable describing the intensity of impact. The nominator represents the amount of momentum delivered by the projectile whereas the denominator represents the flexural resistance of the plate when subjected to impact in the transverse direction.

In Figure 11, the measured values of COR are plotted against the dimensionless impact intensity (as defined by Eq. (18a)). The experimental data points are shown to be distributed following the same trend. A straight line can be approximated in this double logarithmic plot, indicating a power law relationship in Eq. (19), the values of the two coefficients were obtained via the best fitted curve technique.

$$COR = 0.46\left(\frac{(R-r)m_1 v_{10}}{L^2\sqrt{\bar{m}D}}\right)^{-0.144} \quad (19)$$

The value of COR is inferred from experimental measurements to be inversely correlated with the offset of the location of impact from the boundary of the panel, and the amount of momentum delivered by the projectile; but directly correlated with the thickness of the plate (assuming that the material of the plate is homogenous).

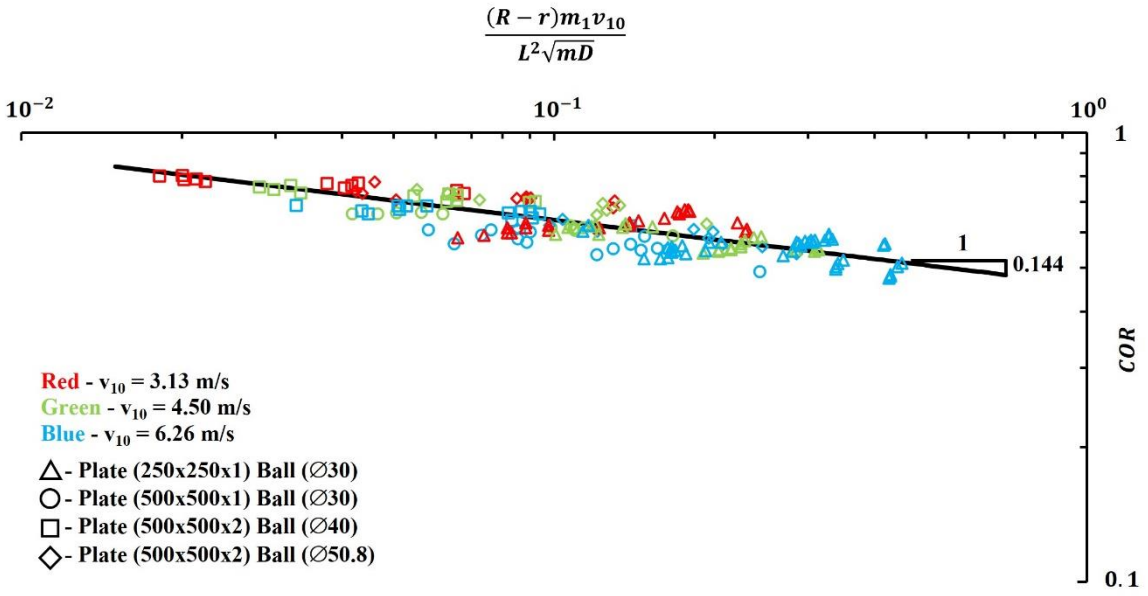


Figure 11: Correlation of coefficient of restitution (COR) with varying impact location defined by $R - r$ (expressed in the dimensionless format)

3.2.3. Permanent indentation w_0

In summary, the analytical prediction of permanent indentation into the plate (w_0) can be determined by use of Eq. (11) when the combinational mass M, the velocity of impact v_{10}, and Coefficient of Restitution COR are well defined. The value of M can be found using Eq. (9) once the value of m_2 is calculated first from Eqs. (16), (17a) or (17b). The amount of permanent indentation into the plate generated in each impact test has also been measured by an optical 3D scanner (*Artec Space Spider 3D*) (refer Figure 12 and 13 which present some scanned images). Good agreement between experimental measurements and analytical predictions across all the tests that have been conducted by the authors is demonstrated as shown in Figure 14.

For each and every group of experiments conducted, results are presented in column charts of different colours (red, blue and green) showing: (1) experimental result, (2) analytical prediction (based on the experimentally measured COR), and (3) analytical prediction (based on the estimated COR calculated by use of Eq. (19)). The comparison between columns (1) and

(2) demonstrates the validity of Eq. (11) whereas the comparison between (2) and (3) further validates accuracy of the empirical relationship of Eq. (19). The numerical discrepancies between (1) and (3) for all the tested groups are within 20%, and with the majority of the results within 10%, as indicated by figures displayed at the respective column chart. Therefore, the accuracy of the proposed analytical model as represented by Eq. (11) and the associated relationships for calculation of M and COR, is validated.

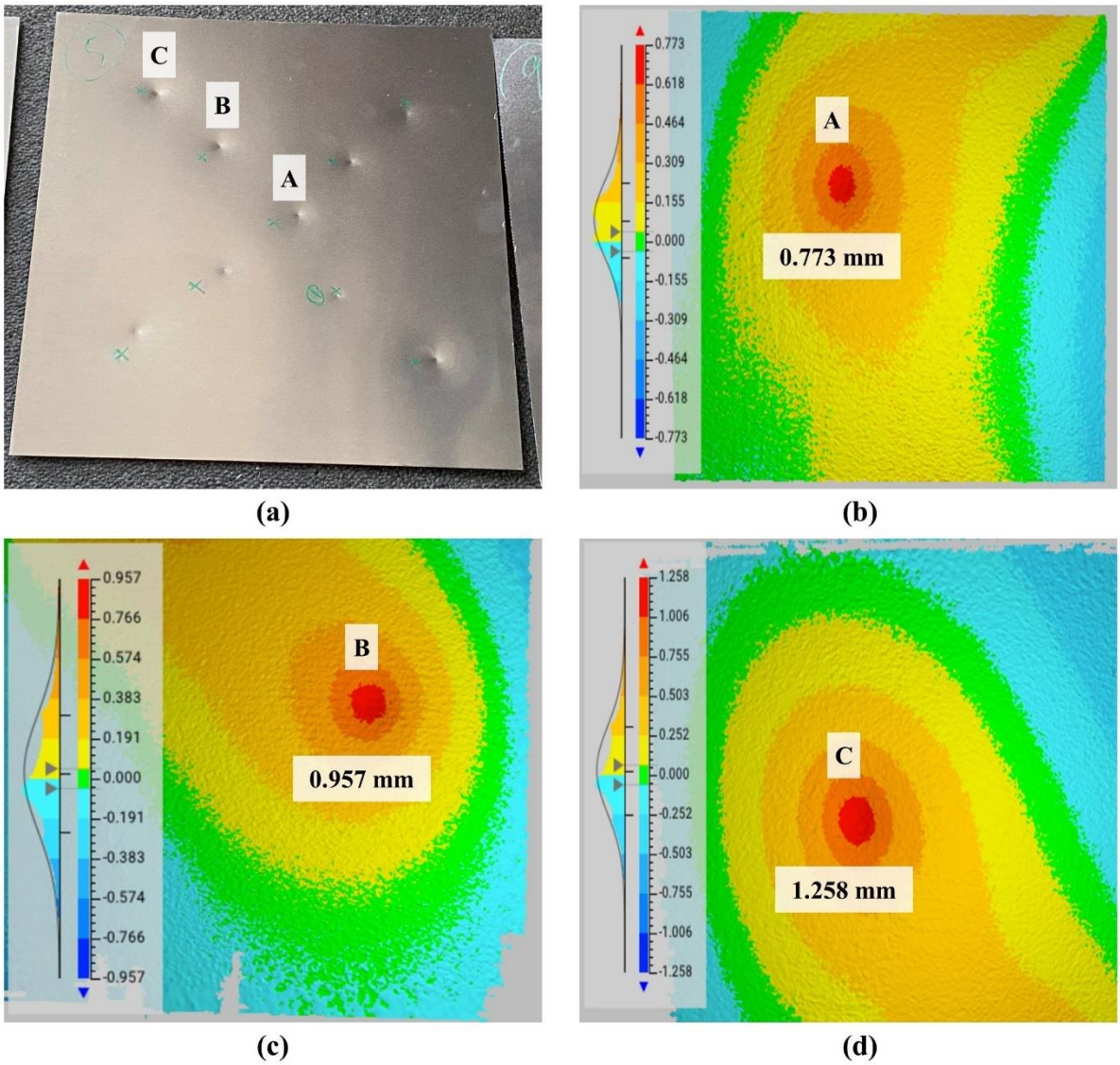


Figure 12: Damage to 250 mm × 250 mm × 1 mm aluminium plate (a) photo of specimen (b) scanned image at point A (c) scanned image at point B (d) scanned image at point C

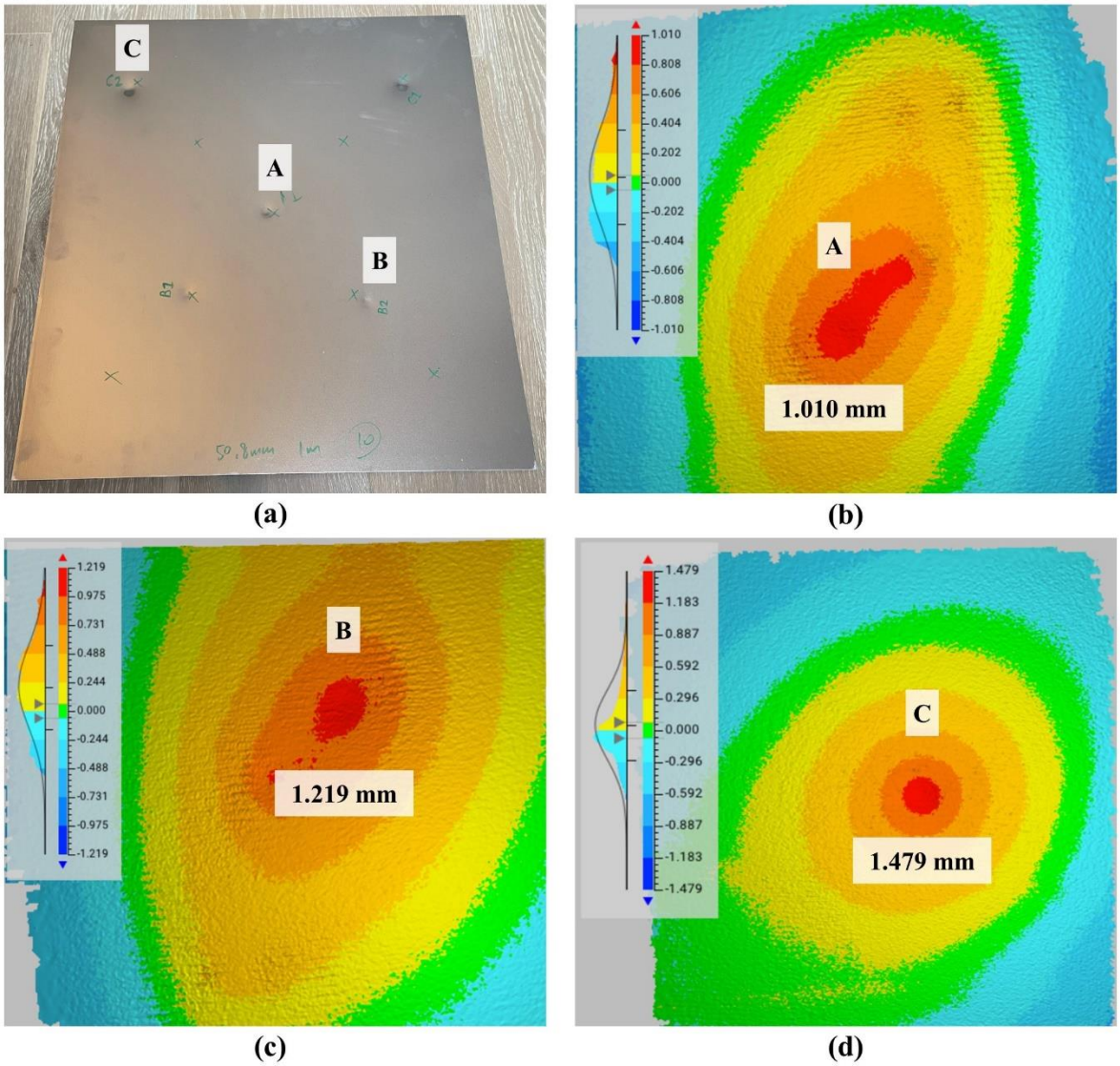
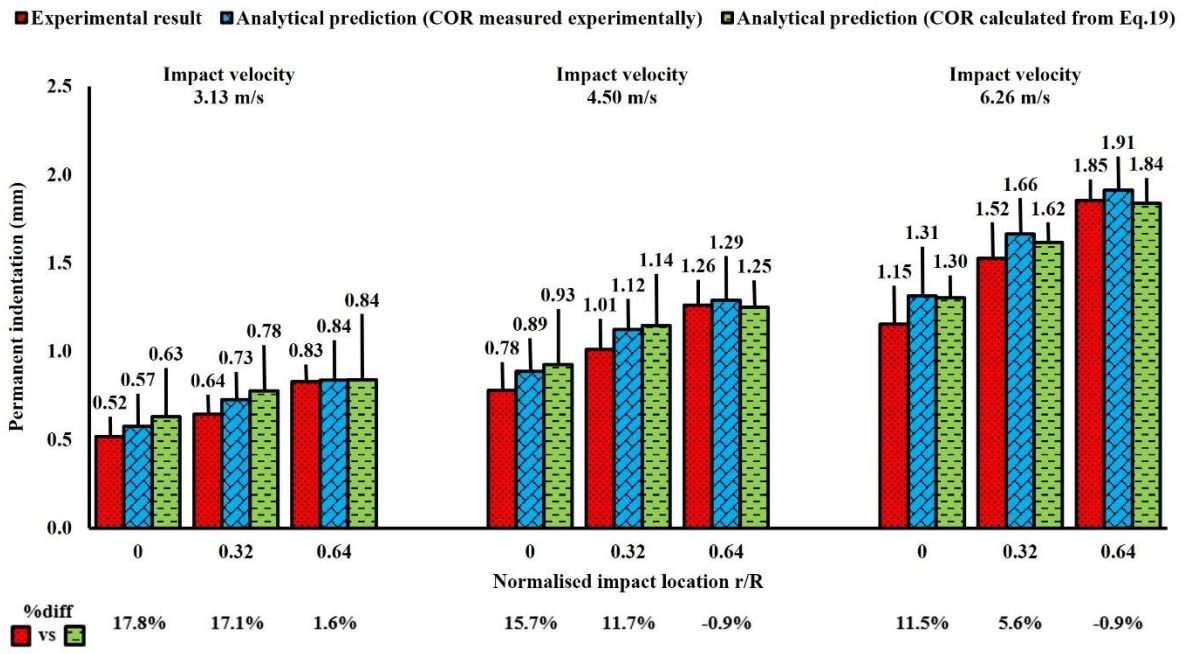
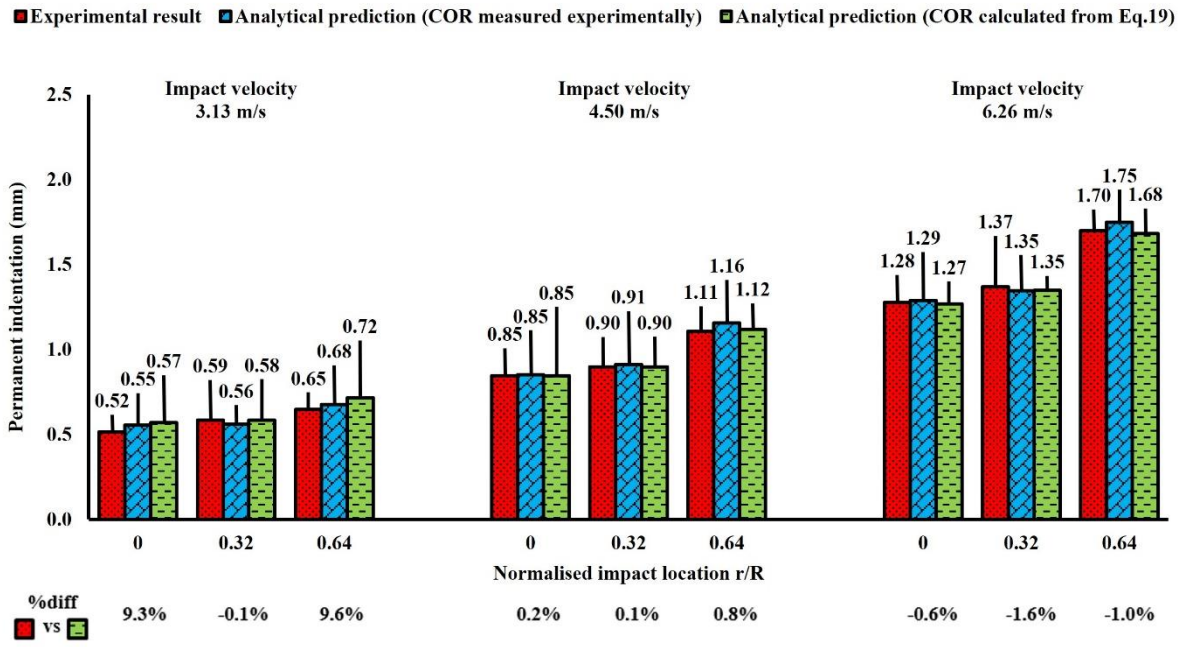


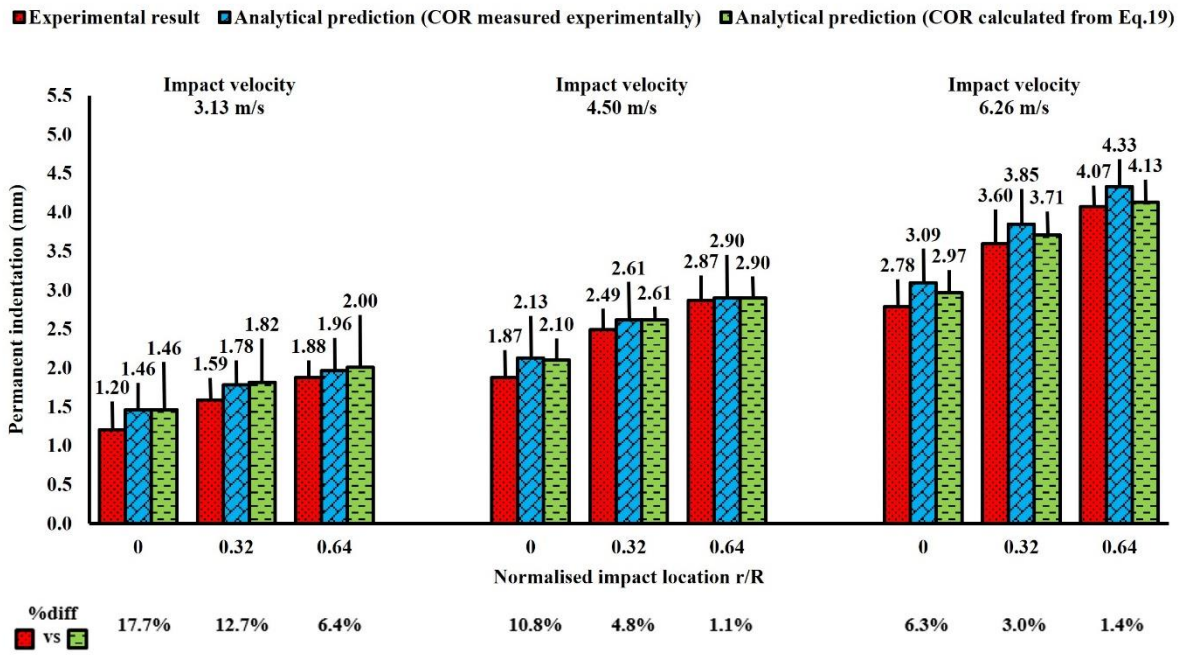
Figure 13: Damage to 500 mm × 500 mm × 2 mm aluminium plate (a) photo of specimen (b) scanned image at point A (c) scanned image at point B (d) scanned image at point C



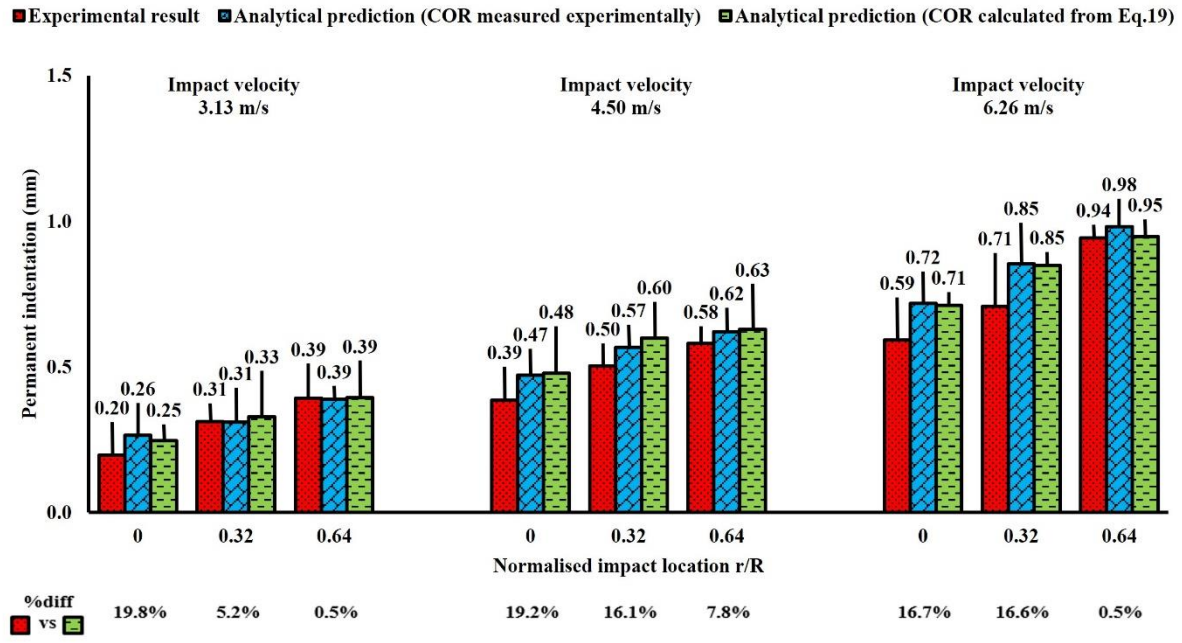
(a) 250 mm × 250 mm × 1 mm plate (30 mm diameter impactor)



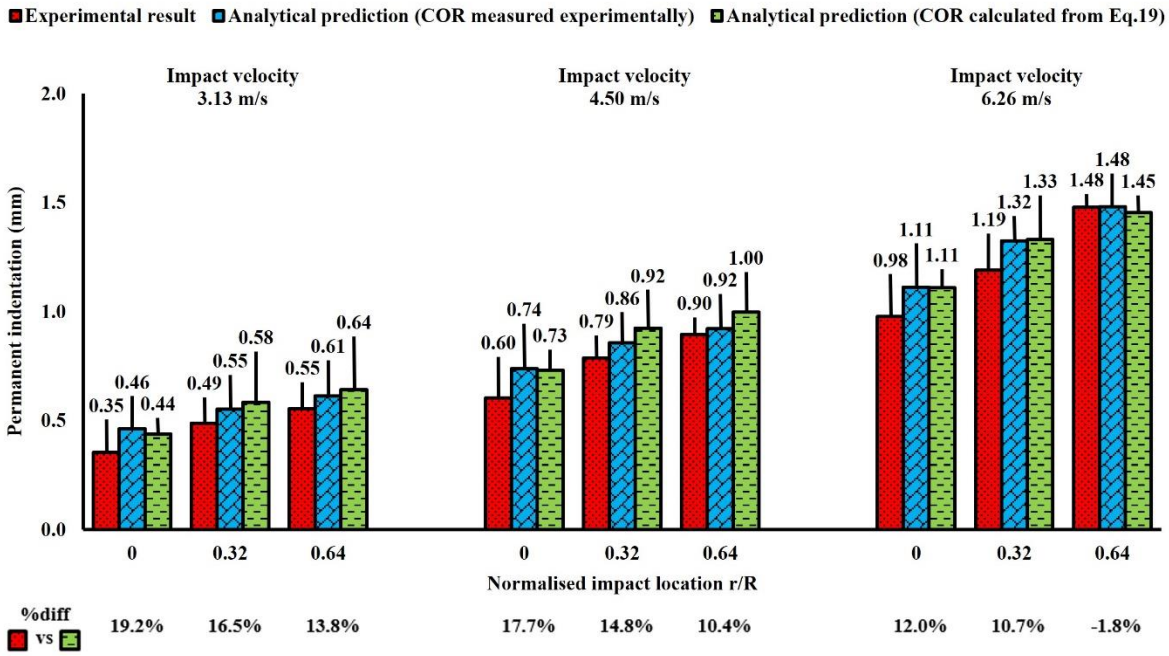
(b) 500 mm × 500 mm × 1 mm plate (30 mm diameter impactor)



(c) 500 mm × 500 mm × 1 mm plate (50.8 mm diameter impactor)



(d) 500 mm × 500 mm × 2 mm plate (50.8 mm diameter impactor)



(e) 500 mm × 500 mm × 2 mm plate (40 mm diameter impactor)

Figure 14: Comparison of permanent indentations predicted by the analytical model and measured by 3D scanner

4. Proposed calculation procedure for prediction of permanent indentation

One of the impact tests conducted by the authors is used herein as example for demonstrating the application of the proposed algebraic predictive relationships. The considered impact scenario was a solid steel sphere impacting at the centre position of an aluminium panel with incident velocity of 6.26 m/s. The targeted panel, which was fully fixed on all the edges, had dimensions of 250 mm × 250 mm × 1mm thick, weighed 158 grams, and was made of alloy type 5050-H34. The impactor was a spherical object made of solid steel of 30 mm in diameter weighting 110 grams. The density, *Poisson's* ratio, Young's modulus, and the yield strength may be taken as 2700 kg/m^3, 0.33, 69 GPa and 140 MPa, respectively. Determine the amount of permanent indentation for the given impact scenario.

Solution:

Step 1 – Solving for participating mass m_2

The participating mass (m_2) of a plate with 1mm thickness when impacted at the centre is predicted by this calculation: $m_2 = \lambda_1 m_1 = \left(0.316\left(\frac{r}{R}\right) + 0.135\right) m_1 = 0.135 \times m_1 = 0.015\ kg$

Step 2 – Solving for combinational mass M

The combinational mass M of the system as given by Eq. (5), is calculated as follows:

$$M = \frac{m_1 m_2}{m_1 + m_2} = \frac{0.11 \times 0.015}{0.11 + 0.015} = 0.013 \text{ kg}$$

Step 3 – Estimating the value of COR

As defined in Eq. (13a), the following parameters need to be calculated first in order to estimate the value of COR:

(a). $R - r = 0.125 \times \sqrt{2} - 0 = 0.177\ m$

(b). $\overline{m} = \rho t = 2700 \times 0.001 = 2.7\ \ kg/m^2$

(c). $D = \frac{Et^3}{12(1-\nu^2)} = \frac{69 \times 10^9 \times (0.001)^3}{12(1-0.33^2)} = 6.45\ Nm^2$

$$COR = 0.46\left(\frac{(R-r)m_1 v_{10}}{L^2\sqrt{\overline{m}D}}\right)^{-0.144} = 0.46\left(\frac{0.177(0.11)(6.26)}{(0.25)^2\sqrt{2.7(6.45)}}\right)^{-0.144} = 0.512$$

Step 4 – Predicting the permanent indentation w_0

Permanent indentation w_0 as estimated from Eq. (7) is shown in below:

$$w_0 = \sqrt{\frac{4}{\pi\sigma_y t} \times \left(\frac{1}{2} M v_{10}^2 (1 - COR^2)\right)}$$

$$= \sqrt{\frac{4}{\pi(140 \times 10^6)(0.001)} \times \left(\frac{1}{2}(0.013)(6.26)^2(1 - 0.512^2)\right)}$$

$$= 0.013 \text{ m or } 1.3 \ mm$$

The predicted value of 1.3 mm can be compared against the experimentally measured value of 1.15 mm demonstrating reasonably good accuracy of the predictive relationships.

5. Conclusion

(i) The algebraic expression for predicting the amount of permanent indentation into the surface of the aluminium has been developed to incorporate the *combinational mass* (M) and the *coefficient of restitution* (COR) as additional input parameters.

(ii) The *participating mass* of the targeted rectangular plate (hence the *combinational mass* of the system) was found to correlate closely with the mass of the impactor; the participating mass ratio (λ) was found to increase with increasing distance from the centre of the plate, and decrease with increasing plate thickness.

(iii) Correlation of the *coefficient of restitution* (COR) with distance from the boundary of the plate and the momentum delivered by the impact has also been identified; and an empirical formula for estimating the value of COR is proposed.

(iv) The accuracy of predictions by the proposed expression has been validated by comparison with results recorded from impact testing which involved dropping a rigid impactor onto aluminium panel specimens of different dimensions.

6. CRediT authorship contribution statement

Shuangmin Shi: Conceptualization, Methodology, Validation, Formal analysis, Investigation, Writing – Original Draft, Visualization. **Nelson Lam:** Conceptualization, Methodology,

Writing – Review & Editing, Supervision. **Yiwen Cui:** Conceptualization, Methodology, Formal analysis. **Lihai Zhang:** Resources, Supervision, Project administration, Funding acquisition. **Guoxing Lu:** Resources, Funding acquisition. **Emad Gad:** Project administration, Funding acquisition.

7. Acknowledgements

Financial support from the Australian Research Council Project LP190100208 titled Performance based assessment of building cladding against hailstorms is acknowledged. Cash and in-kind support by Mr Ian Bennie (General Manager of *Ian Bennie and Associates*) and Mr Suresh Sutrave (Director of *Atlite Skylights*) as Partner Investigators of the linkage project are also gratefully acknowledged.

8. References

1. Changnon, S.A., *Temporal and spatial distributions of damaging hail in the continental United States.* Physical Geography, 2008. **29**(4): p. 341-350.
2. Changnon, S.A., D. Changnon, and S.D. Hilberg, *Hailstorms across the nation: An atlas about hail and its damages.* ISWS Contract Report CR-2009-12, 2009.
3. Minor, J.E., *Windborne debris and the building envelope.* Journal of Wind Engineering and Industrial Aerodynamics, 1994. **53**(1-2): p. 207-227.
4. Sparks, P., *Wind speeds in tropical cyclones and associated insurance losses.* Journal of wind engineering and industrial aerodynamics, 2003. **91**(12-15): p. 1731-1751.
5. Sparks, P.R., S. Schiff, and T. Reinhold, *Wind damage to envelopes of houses and consequent insurance losses.* Journal of wind engineering and industrial aerodynamics, 1994. **53**(1-2): p. 145-155.
6. Standard, B., *Eurocode 1: Actions on structures—*. 2010.
7. Perera, S., et al., *Deterministic solutions for contact force generated by impact of windborne debris.* International Journal of Impact Engineering, 2016. **91**: p. 126-141.
8. Sun, J., et al., *Contact forces generated by fallen debris.* Structural Engineering and Mechanics, 2014. **50**(5): p. 589-603.
9. Sun, J., et al., *Contact forces generated by hailstone impact.* International Journal of Impact Engineering, 2015. **84**: p. 145-158.
10. Sun, J., et al., *Computer simulation of contact forces generated by impact.* International Journal of Structural Stability and Dynamics, 2017. **17**(01): p. 1750005.
11. Sun, J., et al., *A note on Hunt and Crossley model with generalized visco-elastic damping.* International Journal of Impact Engineering, 2018. **121**: p. 151-156.
12. Saini, D. and B. Shafei, *Prediction of extent of damage to metal roof panels under hail impact.* Engineering Structures, 2019. **187**: p. 362-371.
13. Wu, Y., *Determining the effects of hailstone impact on flat cold-reduced steel roof sheeting.* 2018.
14. Saini, D. and B. Shafei, *Design optimization of double-layered structural insulated panels for windborne debris hazard.* Composites Part B: Engineering, 2021. **216**: p. 108806.
15. Saini, D. and B. Shafei, *Performance of structural insulated panels with metal skins subjected to windborne debris impact.* Composites Part B: Engineering, 2020. **198**: p. 108163.
16. Tang, Z., et al., *Numerical and experimental investigation on hail impact on composite panels.* International Journal of Impact Engineering, 2017. **105**: p. 102-108.
17. Tiwari, G., M.A. Iqbal, and P. Gupta, *Energy absorption characteristics of thin aluminium plate against hemispherical nosed projectile impact.* Thin-Walled Structures, 2018. **126**: p. 246-257.
18. Rodriguez-Millan, M., et al., *Perforation mechanics of 2024 aluminium protective plates subjected to impact by different nose shapes of projectiles.* Thin-Walled Structures, 2018. **123**: p. 1-10.

19. Chen, W., H. Hao, and H. Du, *Failure analysis of corrugated panel subjected to windborne debris impacts.* Engineering Failure Analysis, 2014. **44**: p. 229-249.

20. Deb, A., et al., *Numerical Simulation of Projectile Impact on Mild Steel ArmourPlates using LS-DYNA: Part I: Validation.* Defence Science Journal, 2008. **58**(3): p. 422.

21. Herbin, A. and M. Barbato, *Fragility curves for building envelope components subject to windborne debris impact.* Journal of Wind Engineering and Industrial Aerodynamics, 2012. **107**: p. 285-298.

22. Liu, B., R. Villavicencio, and C.G. Soares, *On the failure criterion of aluminum and steel plates subjected to low-velocity impact by a spherical indenter.* International Journal of Mechanical Sciences, 2014. **80**: p. 1-15.

23. Raguraman, M., et al., *Numerical Simulation of Projectile Impact on Mild Steel Armour Platesusing LS-DYNA, Part II: Parametric Studies.* Defence Science Journal, 2008. **58**(4): p. 573.

24. Cheng, Z., et al., *Experiences in reverse-engineering of a finite element automobile crash model.* Finite elements in analysis and design, 2001. **37**(11): p. 843-860.

25. Duffey, T.A., *Large deflection dynamic response of clamped circular plates subjected to explosive loading*. 1967, Sandia Corp., Albuquerque, N. Mex.

26. Alphonso, T. and M. Barbato, *Experimental fragility curves for aluminum storm panels subject to windborne debris impact.* Journal of Wind Engineering and Industrial Aerodynamics, 2014. **134**: p. 44-55.

27. Calder, C.A. and W. Goldsmith, *Plastic deformation and perforation of thin plates resulting from projectile impact.* International Journal of Solids and Structures, 1971. **7**(7): p. 863-881.

28. Mohotti, D., et al., *Out-of-plane impact resistance of aluminium plates subjected to low velocity impacts.* Materials & Design, 2013. **50**: p. 413-426.

29. Pathirana, M., et al., *Damage modelling of aluminium panels impacted by windborne debris.* Journal of Wind Engineering and Industrial Aerodynamics, 2017. **165**: p. 1-12.

30. Shah, Q.H., *Impact resistance of a rectangular polycarbonate armor plate subjected to single and multiple impacts.* International journal of impact engineering, 2009. **36**(9): p. 1128-1135.

31. Shah, Q.H. and Y.A. Abakr, *Effect of distance from the support on the penetration mechanism of clamped circular polycarbonate armor plates.* International Journal of Impact Engineering, 2008. **35**(11): p. 1244-1250.

32. Li, D., et al., *Energy absorption of aluminum panels subjected to gelatin projectile impact.* Latin American Journal of Solids and Structures, 2019. **16**.

33. Hutchings, I., *Energy absorbed by elastic waves during plastic impact.* Journal of Physics D: Applied Physics, 1979. **12**(11): p. 1819.

34. Lankarani, H.M. and P.E. Nikravesh, *Continuous contact force models for impact analysis in multibody systems.* Nonlinear Dynamics, 1994. **5**(2): p. 193-207.

35. Schellenberg, K., *On the design of rockfall protection galleries*. 2008, ETH Zurich.

36. Wu, K. and T. Yu, *Simple dynamic models of elastic–plastic structures under impact.* International journal of impact engineering, 2001. **25**(8): p. 735-754.

37. Yang, Y., N. Lam, and L. Zhang, *Estimation of response of plate structure subject to low velocity impact by a solid object.* International Journal of Structural Stability and Dynamics, 2012. **12**(06): p. 1250053.

38. Corporation, L.S.T., *LS-DYNA Keyword User's Manual Volume II Material Models*. 2021, Livermore Software Technology Corporation Livermore, CA, USA.

39. Corporation, L.S.T., *LS-DYNA Keyword User's Manual Volume I*. 2021, Livermore Software Technology Corporation Livermore, CA, USA.

40. Page, V.A.s.E. *Finite Element Analysis of Structures*. 01/05/2022; Available from: http://www.varmintal.com/aengr.htm#Mats-for-LS-DYNA.

41. Lu, G. and T. Yu, *Energy absorption of structures and materials*. 2003: Elsevier.

42. Stronge, W.J., *Impact mechanics*. 2018: Cambridge university press.

43. Buckingham, E., *On physically similar systems; illustrations of the use of dimensional equations.* Physical review, 1914. **4**(4): p. 345.